Automated Segmentation of Neural Canal Opening and Optic Cup in 3D Spectral Optical Coherence Tomography Volumes of the Optic Nerve Head

Zhihong Hu,[*,1] *Michael D. Abràmoff,*[1,2,3] *Young H. Kwon,*[2] *Kyungmoo Lee,*[1] *and Mona K. Garvin*[*,1]

Purpose. To develop an automated approach for segmenting the neural canal opening (NCO) and cup at the level of the retinal pigment epithelium (RPE)/Bruch's membrane (BM) complex in spectral-domain optical coherence tomography (SD-OCT) volumes. To investigate the correspondence and discrepancy between the NCO-based metrics and the clinical disc margin on fundus photographs of glaucoma subjects.

Methods. SD-OCT scans and corresponding stereo fundus photographs of the optic nerve head were obtained from 68 eyes of 34 patients with glaucoma or glaucoma suspicion. Manual planimetry was performed by three glaucoma experts to delineate a reference standard (RS) for cup and disc margins from the images. An automated graph-theoretic approach was used to identify the NCO and cup. NCO-based metrics were compared with the RS.

Results. Compared with the RS disc margin, the authors found mean unsigned and signed border differences of 2.81 ± 1.48 pixels (0.084 ± 0.044 mm) and −0.99 ± 2.02 pixels (−0.030 ± 0.061 mm), respectively, for NCO segmentation. The correlations of the linear cup-to-disc (NCO) area ratio, disc (NCO) area, rim area, and cup area of the algorithm with the RS were 0.85, 0.77, 0.69, and 0.83, respectively.

Conclusions. In most eyes, the NCO-based 2D metrics, as estimated by the novel automated graph-theoretic approach to segment the NCO and cup at the level of the RPE/BM complex in SD-OCT volumes, correlate well with RS. However, a small discrepancy exists in NCO-based anatomic structures and the clinical disc margin of the RS in some eyes. (*Invest Ophthalmol Vis Sci.* 2010;51:5708–5717) DOI:10.1167/iovs.09-4838

Glaucoma is a chronic neurodegenerative disease of the optic nerve that, if left untreated, may result in increasing visual field (VF) loss and blindness. It is characterized by the degeneration of the retinal ganglion cell axons.[1,2] It has been suggested that the initial axonal insult occurs in the optic nerve head (ONH), which leads to optic disc cupping and VF loss through retinal ganglion cell apoptosis.[1] The risk for VF loss from glaucoma can be minimized by early diagnosis and careful monitoring of disease progression. However, the latter requires a reproducible measurement of the disease state. Currently available methods include VF, planimetry based on stereo disc photographs, ONH tomography (Heidelberg Retina Tomograph; Heidelberg Engineering, Heidelberg, Germany), and peripapillary nerve fiber layer thickness analysis (using polarimetry or optical coherence tomography [OCT]).[3–7] Many of these modalities involve a subjective component, by either the patient or the examiner, which can decrease reproducibility.

Spectral domain optical coherence tomography (SD-OCT) is a relatively new modality that provides a cross-sectional, microscale depiction of the optical reflectance properties of the biological tissues.[8] The high-resolution SD-OCT scans of the ONH provide a potential to identify glaucomatous changes using 3D information. However, it is unclear which ONH parameters derived from SD-OCT can be best used to quantify glaucomatous changes.

We have recently described a voxel classification approach for automatically segmenting the clinically familiar glaucomatous parameters—the ONH rim and cup—directly from the SD-OCT volumes[9] by extending our previous approach for automated planimetry on stereo fundus photographs.[10,11] However, this approach has the ultimate limitation in that the algorithm essentially mimics the subjective assessment of 2D parameters by human experts. It is not based on objective anatomic landmarks within the 3D volumes, and we have found that the optic disc margin does not overlap with a single constant anatomic structure in volumetric OCT, consistent with the recent comparisons of clinical and SD-OCT optic disc margin anatomy by Strouthidis et al.[12,13] They found that the varying combinations of the termination of Bruch's membrane (BM), border tissue, or the anterior scleral canal opening may manifest as the 2D disc margin seen on photographs, depending on the border tissue architecture and anatomy.

Given the wealth of volumetric information available with SD-OCT, it is likely that better parameters can be obtained for measuring glaucomatous change that move beyond what is possible using stereo fundus photography alone. A central requirement for the detection of the ONH structural change is a longitudinally stable zero reference plane. As described by Strouthidis et al.,[12,13] the neural canal opening (NCO)—the termination of the RPE/BM complex—can serve as a basis for a stable reference plane from which various optic nerve morphometric parameters can be derived, based on the assumption that the NCO is not likely to change substantially with glaucomatous progression.[12,13]

From the [1]Department of Electrical and Computer Engineering, University of Iowa, Iowa City, Iowa; the [2]Department of Ophthalmology and Visual Sciences, University of Iowa Hospitals and Clinics, Iowa City, Iowa; and the [3]Department of Veterans Affairs, Iowa City VA Medical Center, Iowa City, Iowa.

Supported by National Institutes of Health Grants EY017066 and EB004640, Research to Prevent Blindness, the Department of Veterans' Affairs, and the Marlene S. and Leonard A. Hadley Glaucoma Research Fund.

Submitted for publication October 28, 2009; revised April 14 and May 18, 2010; accepted May 25, 2010.

Disclosure: **Z. Hu**, None; **M.D. Abràmoff**, P; **Y.H. Kwon**, P; **K. Lee**, None; **M.K. Garvin**, P

*Each of the following is a corresponding author: Zhihong Hu, 4016 Seamans Center, University of Iowa, Iowa City, IA 52242; zhihong-hu@uiowa.edu.

Mona K. Garvin, 4318 Seamans Center, University of Iowa, Iowa City, IA; mona-garvin@uiowa.edu.

Investigative Ophthalmology & Visual Science, November 2010, Vol. 51, No. 11

Thus, the core hypothesis motivating our present study is that the segmentation of a stable 3D structure, the NCO, from SD-OCT will enable more reproducible and objective glaucomatous parameters than are currently possible from manual planimetry alone (even using a consensus of glaucoma experts). This is fundamentally different from our previous segmentation method,[9] which, by construction (using training data), attempts to obtain parameters as close as possible to what would be obtained using manual planimetry of stereo fundus photographs. Although the present study does not directly test this hypothesis, it sets the necessary underlying framework for the ability to automatically detect the NCO and to better understand its relationship with the widely accepted optic disc margin from manual planimetry.

More specifically, the purpose of the present study was to describe an algorithm for automatic delineation of the NCO from SD-OCT volumes and optic disc metrics derived from the NCO (and cup boundaries) and to compare these with the reference standard (RS; disc and cup margins) obtained from human expert planimetry of stereo photographs of the same eye.

Patients, Materials, and Methods

Patients

Thirty-four consecutive patients with the diagnosis of glaucoma suspect, open-angle glaucoma, angle-closure glaucoma, or combined-mechanism glaucoma from the Glaucoma Clinic at the University of Iowa were included in this study.[9] Nonglaucomatous optic neuropathy was excluded. The patient cohort has been described in detail in a previous report.[9] Diagnoses were made by the treating glaucoma specialist. The study was approved by the Institutional Review Board of the University of Iowa and adhered to the tenets of the Declaration of Helsinki, and all subjects gave written informed consent.

Image Acquisition

Sixty-eight ONH-centered SD-OCT scans of the 34 consecutive study subjects were acquired using a spectral domain OCT device (Cirrus; Carl Zeiss Meditec, Inc., Dublin, CA). The OCT scans were exported in an uncompressed raw format (40 Mb/scan), preserving the voxel intensities. Each SD-OCT scan consisted of $200 \times 200 \times 1024$ voxels, and the physical dimensions were $6 \times 6 \times 2$ mm^3. Thus, the voxel resolution was $30 \times 30 \times 2$ μm.[9] The voxel depth was 8 bits in grayscale. Sixty-eight corresponding stereo color fundus photographs of the optic disc were also acquired on the same day using a stereo retinal camera (3Dx; Nidek, Newark, NJ) with a fixed stereo base with a digital camera back (Nidek). The size of the stereo color fundus disc photographs was 4096×4096 pixels, and the pixel depth was $3 \times$ 8-bit in red, green, and blue channels.

OCT Volume Flattening

Because of the shape of the globe, the scanner position relative to the patient's pupil, and the eye movement, the original raw OCT image was deformed elastically. Thus, four intraretinal surfaces were segmented in 3D[14,15] and the raw OCT volume was flattened based on the second segmented surface, as described previously.[16] From top to bottom (Figs. 1b, 1e), surface 1 corresponded to the internal limiting membrane (ILM), surface 2 was located between the inner and outer segments of the photoreceptors, surface 3 was the inner boundary of the RPE/BM complex, and surface 4 was the outer boundary of the RPE/BM complex. Surface 2 was chosen as the flattening surface (in this stage) for consistency with our previous work[15]; however, surface 3 would have worked equally well in this flattening stage because one of its major purposes was only to remove the motion artifacts across B-scans to make the NCO and cup segmentation easier. As shown in Figures 1c and 1f, the geometric distortion across B-scans was improved, though not perfect, after the flattening. Flattening also pro-

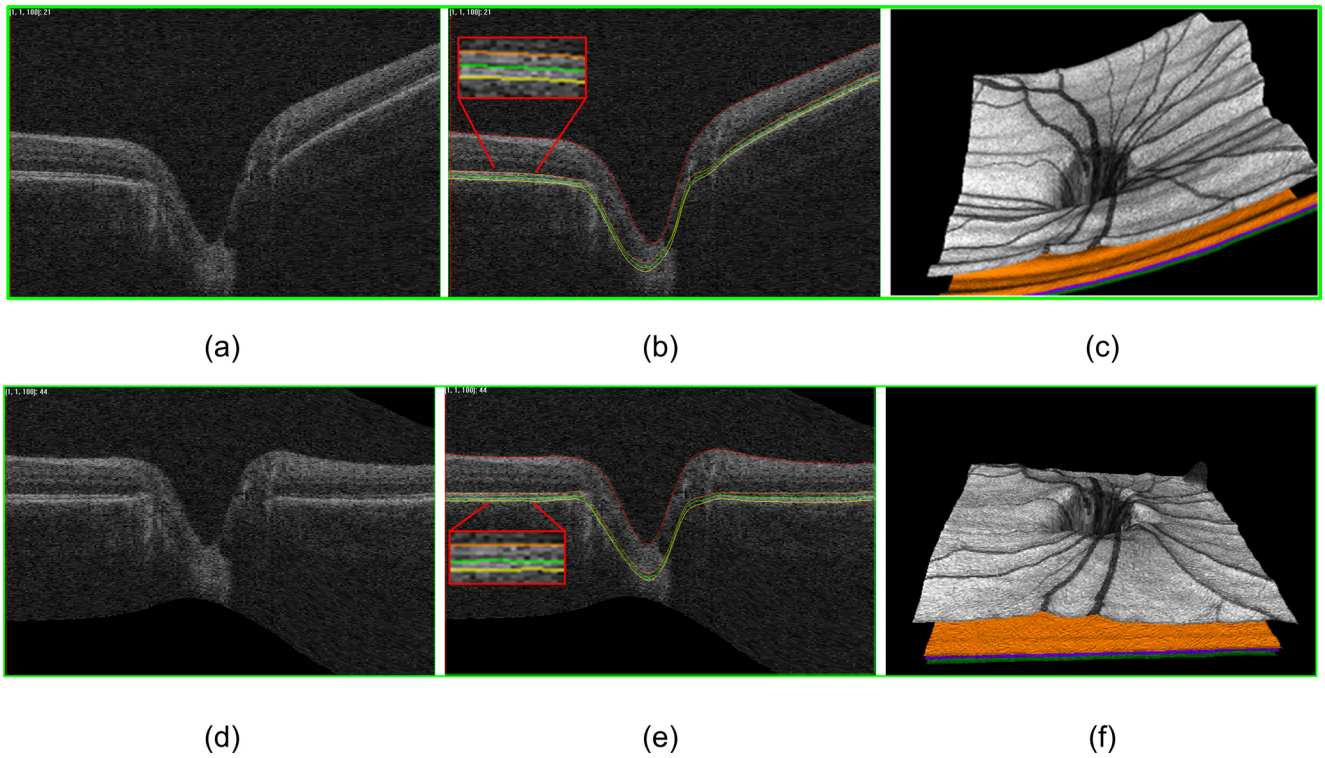

Figure 1. Illustration of SD-OCT volume flattening. (**a**) Central slice from the original raw SD-OCT. (**b**) Four surface segmentations of the original raw volume. (**c**) 3D rendering of the surface segmentation by mapping of the projection image texture onto the top surface. (**d**) Central slice from the flattened SD-OCT. (**e**) Four surface segmentations of the flattened volume. (**f**) 3D rendering of the surface segmentation of the flattened volume by mapping the projection image texture onto the top surface.

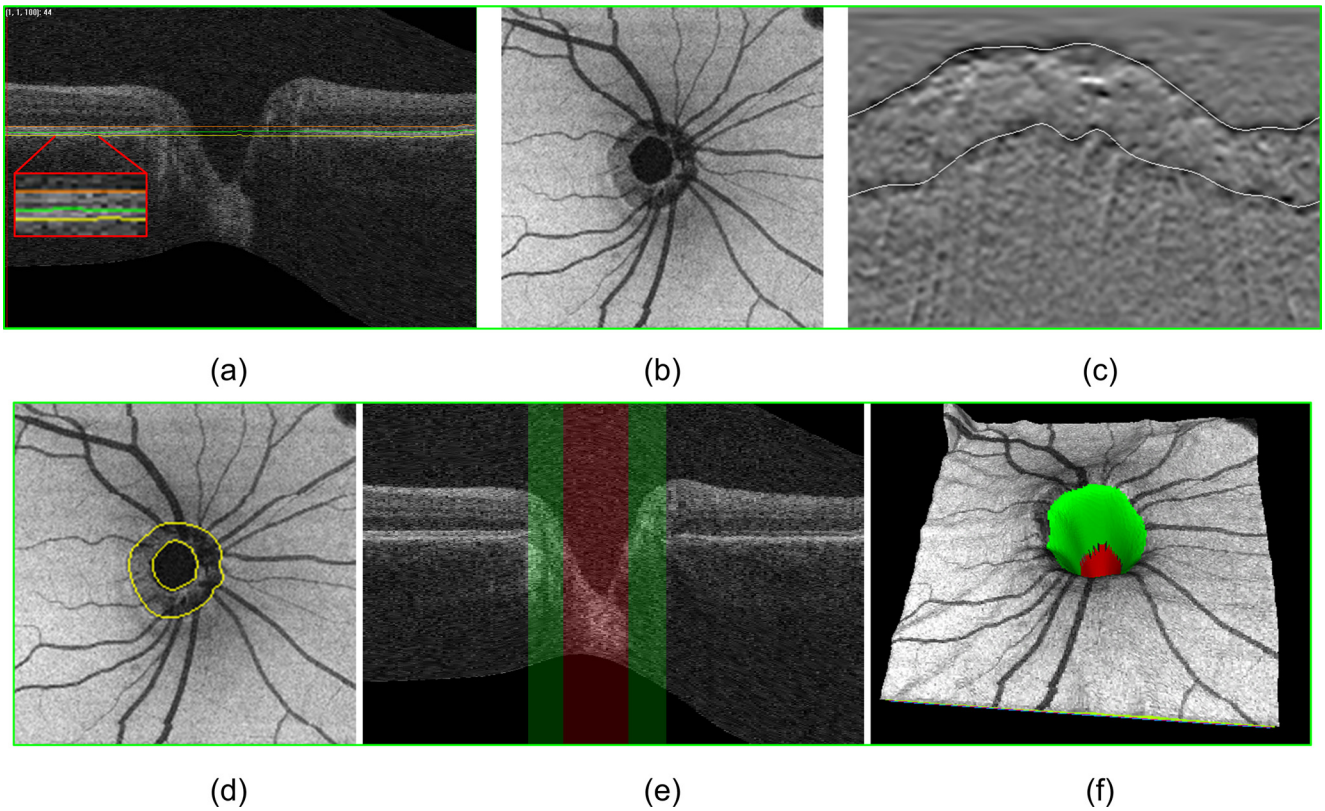

FIGURE 2. Illustration of the NCO and optic cup segmentation at the RPE/BM plane. (**a**) Planar surfaces near RPE/BM complex. (**b**) Projection image. (**c**) Segmented boundaries overlapping with the unwrapped cost image. (**d**, **e**) Segmented NCO and cup overlapping with (**d**) projection image and (**e**) cross-sectional slice of OCT volume. (**f**) 3D rendering of the NCO and cup segmentation overlapping with the mapping of the projection image texture onto the top surface.

vided a possibility to create a projection image from a thin layer at the RPE/BM complex for correspondingly comparing the NCO-based parameters with those of fundus photographs.

NCO and Optic Cup Segmentation at the RPE/BM Plane

Because of the large variations in the surface of the ONH, intraretinal layer segmentation differences can occur and cause a nonoptimal flattening problem (i.e., the NCO points do not lie on a plane after flattening). Therefore, we first established an estimated NCO region, a circular region centered on the geometric center of the OCT volume with a radius certain to be larger than the estimated NCO boundary. A projection image (Hu Z, et al. *IOVS* 2009;50:ARVO E-Abstract 3334) was formed by taking the thin layer between surface 2 (orange) and surface 4 (yellow; Fig. 2a) and by extrapolating the average position outside the estimated NCO region for surfaces 2, 3, and 4 to the inside region radially. The outer boundary in the projection image (Fig. 2b) corresponded to the NCO, and the inner boundary corresponded to the cup at the level of the RPE/BM plane.

We then transformed the projection image to polar coordinates by unwrapping from the center of the projection image. A signed edge-based term, favoring a dark-to-bright transition in the vertical direction (Fig. 2c) from the transformed projection image, was used as the cost function, and we modeled the resultant cost image as a weighted, directed graph similar to the one described by Li et al.[17] We used a graph search to simultaneously segment the (optimal) NCO and cup boundaries.[18] In shallow cups (or if the cup was absent), the deepest point of the top surface did not extend below the level of the RPE/BM plane (Fig. 2a, green). When this occurred, the algorithm automatically switched from using a two-boundary graph search to using a one-boundary graph search so that the NCO was determined using the single-boundary graph search method. The NCO and cup boundaries were finally smoothed using a B-spline.

Comparison of the Algorithm with Expert Planimetry Stereo Color Photographs

Computer-aided planimetry was performed by three fellowship-trained glaucoma experts on stereo color photographs of the optic disc, as

TABLE 1. NCO Border Positioning Differences from the 68 Eyes

Difference	Algorithm vs. RS*	Expert 1 vs. 2†	Expert 1 vs. 3†	Expert 2 vs. 3†
Mean unsigned, pixel	2.81 ± 1.48	3.82 ± 1.48	3.39 ± 1.65	2.06 ± 0.95
Mean unsigned, mm	0.084 ± 0.044	0.115 ± 0.045	0.102 ± 0.049	0.062 ± 0.028
Mean signed, pixel	−0.99 ± 2.02	−2.52 ± 1.40	−1.18 ± 1.14	1.36 ± 1.42
Mean signed, mm	−0.030 ± 0.061	−0.075 ± 0.042	−0.035 ± 0.034	0.041 ± 0.043

* Mean unsigned and signed border positioning differences between the automated NCO segmentation and the optic disc segmentation of the RS.

† Interobserver variability.

TABLE 2. Correlations of the Algorithm with the Expert Segmentation from the 68 Scans

Correlation	Algorithm vs. RS*	Expert 1 vs. 2†	Expert 1 vs. 3†	Expert 2 vs. 3†
LCDR	0.85 (0.76~0.90)	0.88 (0.82~0.93)	0.92 (0.87~0.95)	0.88 (0.81~0.93)
Disc area	0.77 (0.64~0.85)	0.86 (0.79~0.92)	0.91 (0.87~0.95)	0.88 (0.81~0.92)
Rim area	0.69 (0.55~0.80)	0.78 (0.66~0.86)	0.84 (0.75~0.90)	0.80 (0.69~0.87)
Cup area	0.83 (0.73~0.89)	0.93 (0.88~0.95)	0.95 (0.91~0.97)	0.90 (0.85~0.94)

Values in parentheses are 95% confidence intervals.

* Correlations of NCO, rim, and cup at RPE/BM plane from the algorithm with disc, rim, and cup from RS, respectively.

† Correlations between different expert segmentations.

described previously.[9] RS was obtained from the three expert segmentations on the color fundus image based on consensus (each pixel was assigned a class that received the majority of votes). For example, if two votes were for a pixel to be rim and one vote was for a pixel to be cup, the pixel was assigned to rim.[9,15] The linear cup-to-disc area ratio (LCDR) was defined as the square root of the cup area over disc area.

To determine the transformation necessary to convert the expert segmentations on the stereo color fundus images to the SD-OCT space, manual registration was performed as described previously.[9] More specifically, a projection image was created by averaging the voxels between the second and fourth intraretinal surfaces (Fig. 1e, orange and yellow lines). Note that this projection image was different from the projection images created for finding the NCO. The goal of creating this projection image was to obtain the RS for OCT scans and was referred to as RS-aimed projection image. The manual registration was performed by matching blood vessels between the stereo retinal fundus images and the corresponding RS-aimed projection images. The RS and the three expert segmentations from the stereo fundus images were also converted to the SD-OCT space by applying the same transformation.[9,15]

The algorithm NCO boundary was compared with the RS disc margin using mean unsigned and signed border differences (the closest Euclidean distances between the segmented NCO points from our algorithm and those from the RS and vice versa). Signed difference was measured in terms of the disc center of the RS. If the distance of the NCO points to the disc center of the RS was greater than that of the optic disc margin of the RS to its center, the signed difference was positive, and vice versa.

The algorithm was also compared with the RS in terms of the correlations of linear cup-to-NCO/cup-to-disc area ratio, cup area, rim area, and NCO/disc area. Interobserver correlations of the same parameters were investigated.

RESULTS

Table 1 shows the mean border positioning differences of the NCO with the optic disc from the RS for the 68 eyes of the 34 patients. The mean unsigned and signed differences of the

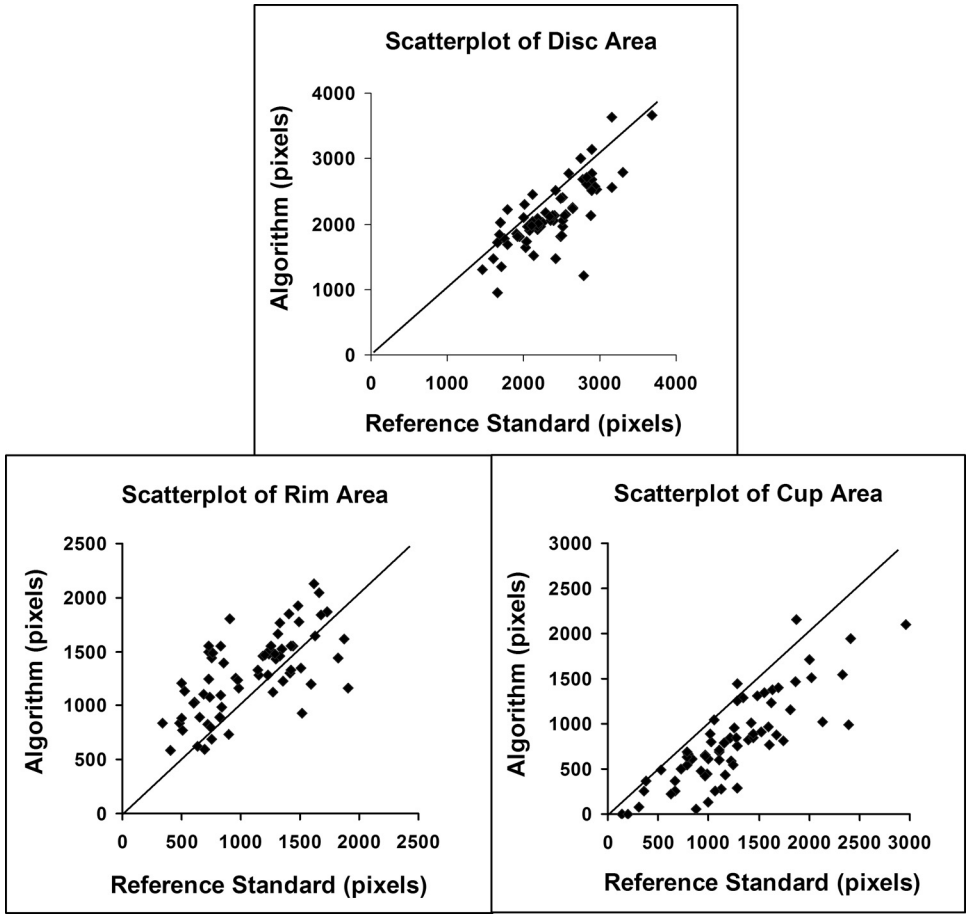

FIGURE 3. Scatterplots of the NCO, rim, and cup area at the RPE/BM plane from the algorithm to the disc, rim, and cup area from RS for the 68 eyes. *Diagonal line*: perfect correlation of 1.0.

algorithm with the RS for 68 eyes were 2.81 ± 1.48 pixels (0.084 ± 0.044 mm) and −0.99 ± 2.02 pixels (−0.030 ± 0.061 mm), respectively.

Table 2 compares the algorithm segmentation results of the 68 eyes with the RS in terms of the correlations with the confidence intervals (CIs) for the linear cup-to-NCO/cup-to-disc area ratio, NCO/disc area, rim area, and cup area. The correlations of the linear cup-to-NCO/cup-to-disc area ratio, NCO/disc area, rim area, and cup area of the algorithm with the RS for the 68 eyes were 0.85, 0.77, 0.69, and 0.83, respectively.

The scatterplots of the NCO/disc area, rim area, and cup area are illustrated in Figure 3. The scatterplots of the LCDR and the interobserver variability are illustrated in Figure 4, with the perfect correlation line indicated as a reference. As seen in Figure 3, the algorithm NCO area is similar to the disc area of the RS, the rim tends to run slightly greater than that of the RS, and the cup tends to run slightly smaller than the RS cup. Correspondingly, the algorithm LCDR is slightly smaller than that of the RS (Fig. 4).

Although the 68 eye analyses were performed to obtain additional statistical power, we also computed the border positioning differences and the correlations of the measured metrics by randomly choosing one eye from each of the 34 patients. The mean border positioning differences were 2.68 ± 1.14 pixels (0.080 ± 0.034 mm) and −0.74 ± 1.76 pixels (−0.022 ± 0.053 mm), respectively, similar to the 68 eye results. Correlations of the measured metrics for the 34 eyes were also similar to those of the 68 eyes.

Figure 5 shows the algorithm segmentation from seven right eyes of seven randomly chosen patients. The right eye was chosen simply for ease of display (the left eye showed similar results). Each row corresponds to an eye.

Based on the quantitative results and qualitative visual inspection, there was a reasonable match in most eyes between the algorithm's objectively determined NCO and cup and the glaucoma expert's subjectively determined disc margin and cup of the RS.

Figures 6, 7, and 8 visually demonstrate three segmentation comparisons of our present and previous algorithms[9] and the RS overlapping with the transformed fundus image and the SD-OCT volume. More specifically, Figure 6 is an example demonstrating a good match between the three approaches. Figures 7 and 8 are two examples demonstrating a discrepancy between the present algorithm,the previous algorithm, and the RS overlapping with the transformed fundus image and the SD-OCT volume. The previous algorithm and the RS segment the clinically appreciable defined optic disc margin. The present algorithm instead segments the true SD-OCT–based anatomic structures (NCO and optic cup at the RPE/BM complex). Based on these examples, one can clearly see the sources of the small discrepancies of the NCO and the clinical optic disc, though in most scans, the NCO demonstrates a good match with the clinically appreciable defined optic disc margin obtained by planimetry.

Discussion

In this study, we present an algorithm to automatically segment the NCO and optic cup at the RPE/BM plane in SD-OCT volumes. Using human expert planimetry on the stereo photographs as the RS, we showed that the NCO border positioning differences (Table 1) between the algorithm and the RS for the

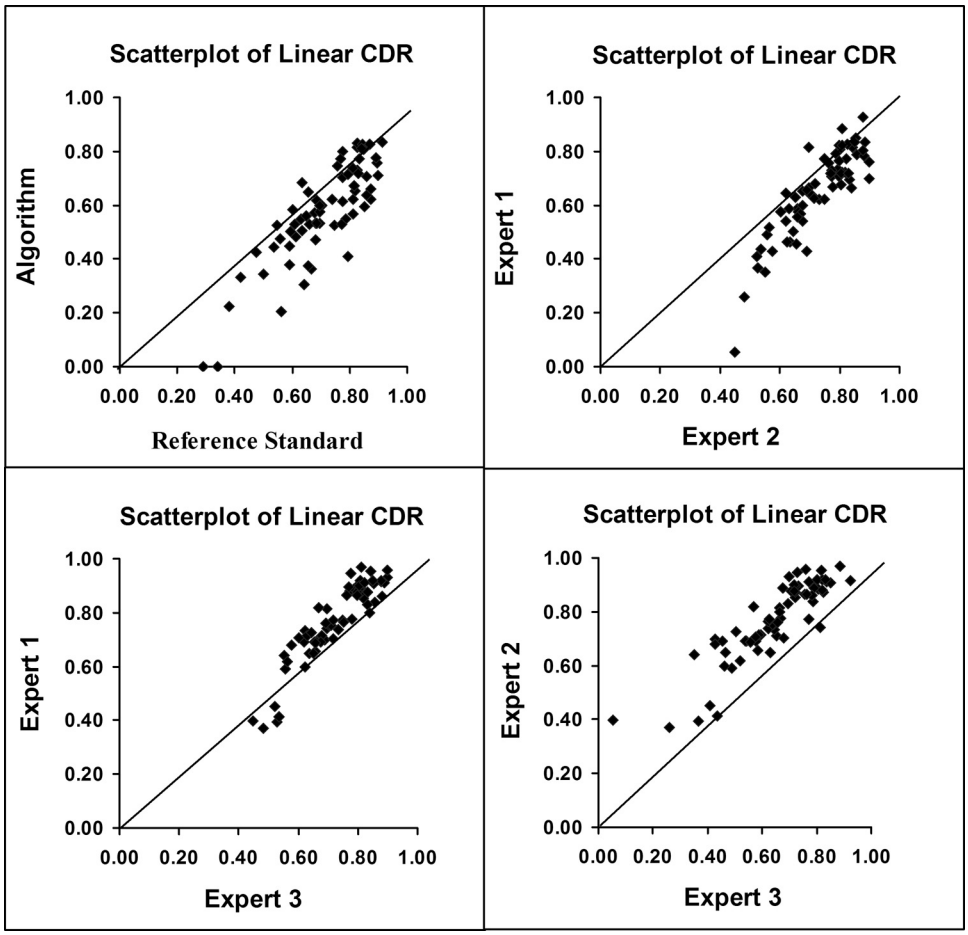

Figure 4. Scatterplots of linear cup-to-NCO of algorithm to LCDR of RS for 68 eyes. *Diagonal line*: perfect correlation of 1.0.

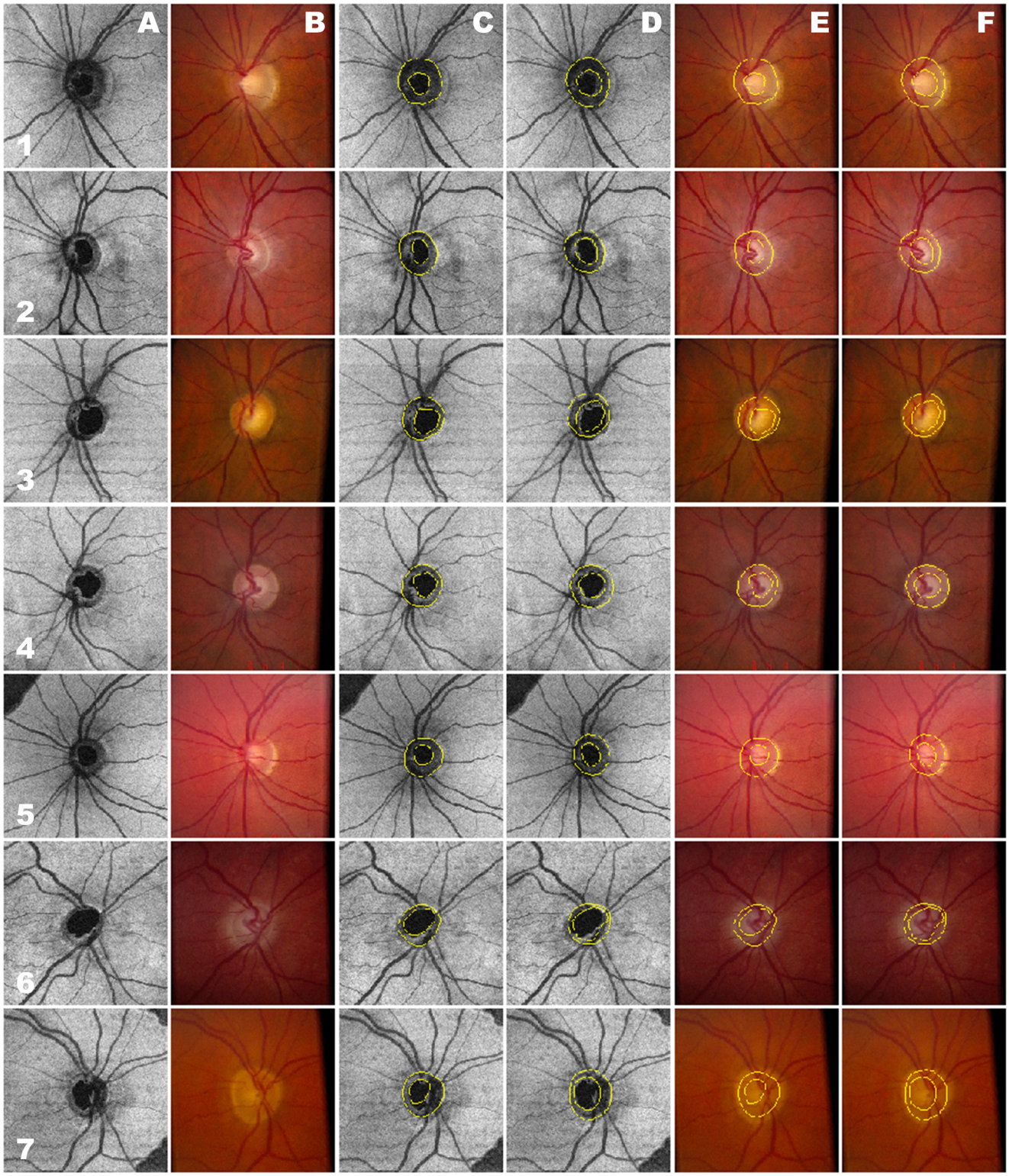

FIGURE 5. Random selection of example NCO segmentations. (**A**) Projection image. (**B**) Corresponding fundus image. (**C**, **D**) NCO and cup at RPE/BM plane from present algorithm and disc and cup from RS transposed to projection image, respectively. (**E**, **F**) NCO and cup at RPE/BM plane from present algorithm and disc and cup from RS transposed to fundus image, respectively.

68 eyes were as good as interobserver differences. The linear cup-to-NCO area ratio (Table 2) for the 68 eyes correlated reasonably well with the LCDR of the RS (r = 0.85). Other objectively derived 2D SD-OCT metrics (Table 2) correlated reasonably well with those of the RS (r = 0.69~0.83). In addition, we qualitatively (Figs. 5, 6) demonstrated the good match of the present algorithm and the RS. We concluded that in most eyes the NCO in SD-OCT was consistent with the clinically appreciable defined optic disc margin obtained by planimetry.

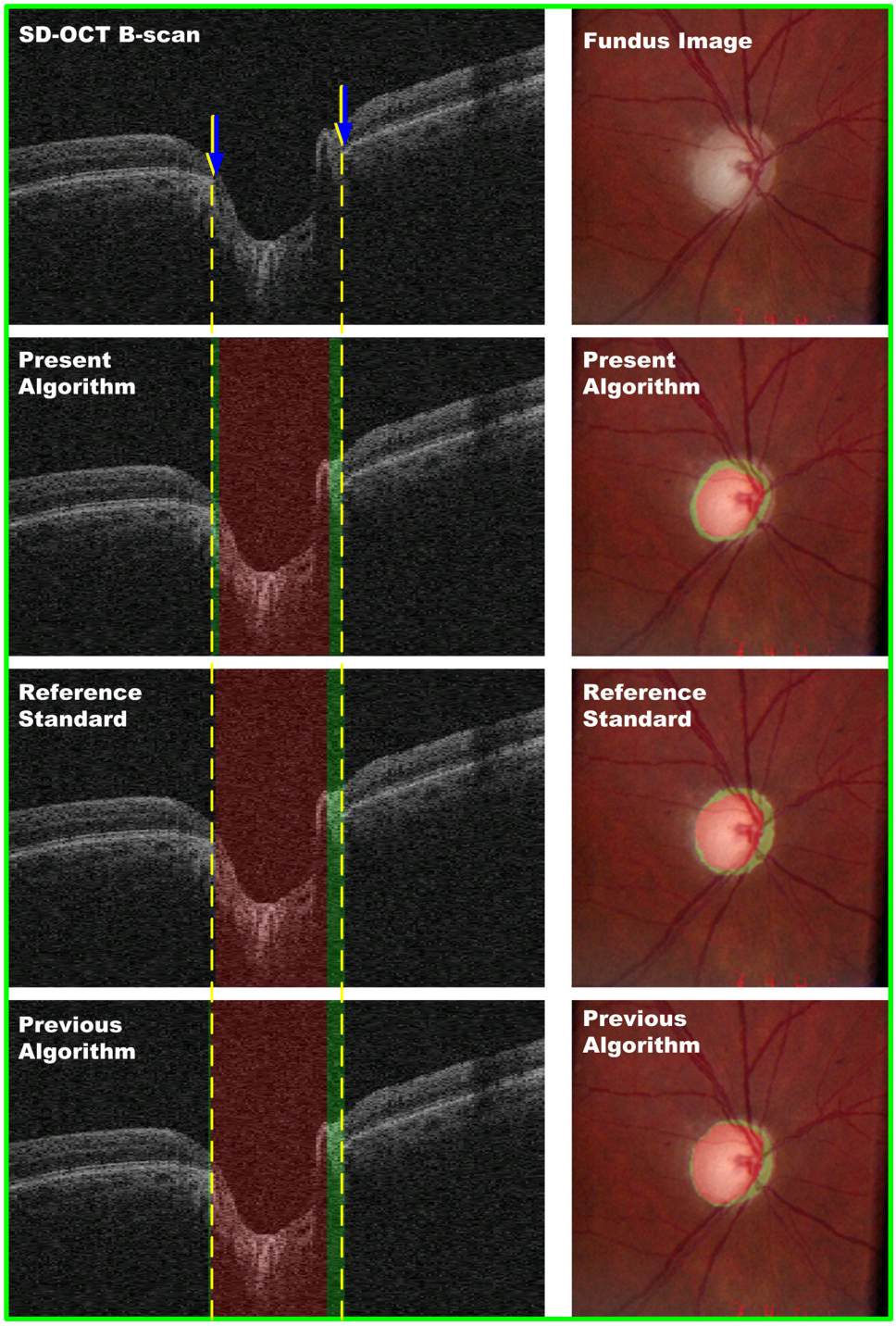

Figure 6. Comparison of present algorithm, expert, and previous algorithm segmentations with a good match. Raw SD-OCT and corresponding fundus image (*row 1*), present algorithm (*row 2*), RS (*row 3*), and previous algorithm (*row 4*) segmentations overlapping with raw SD-OCT and corresponding fundus image. SD-OCT central B-scan (*left*) and fundus image (*right*). *Yellow arrows*: position of the NCO from the algorithm (*dashed yellow line* indicates the projected NCO position). *Blue arrows*: clinical disc from the RS. *Green*, *red*: each method's projected rim and cup regions, respectively.

However, even though the NCO boundary and clinical disc margin corresponded reasonably well in most eyes, it is interesting to note the discrepancies (Figs. 7, 8). These discrepancies were consistent with the findings reported by Strouthidis et al.[12,13] In particular, we found that the clinical disc margin sometimes corresponded with the varying combinations of different structures other than the NCO, such as the border tissue of Elschnig. For instance, in the SD-OCT B-scan shown in Figure 7, the RS defined the innermost termination of the border tissue as the temporal optic disc margin (blue arrow). In Figure 8, the RS defined the border tissue as the temporal optic disc margin (blue arrow), which was obviously different from the NCO (yellow arrow) of the algorithm.

Because of such underlying differences, compared with the parameter correlations by planimetry between different experts, the relatively smaller correlations of the NCO-based metrics with those of the RS (Table 2) were not surprising. However, the fact that the algorithm demonstrated smaller unsigned border positioning differences than those between the experts (Table 1) yet had lower correlations (Table 2) was surprising. This might have occurred in part because correlation (measuring the direction and noise of linear relationships) does not take into account any bias (e.g., consistent overestimation or underestimation of a parameter), whereas the unsigned border positioning errors were influenced by any bias between the measurements. Given that the experts tended to

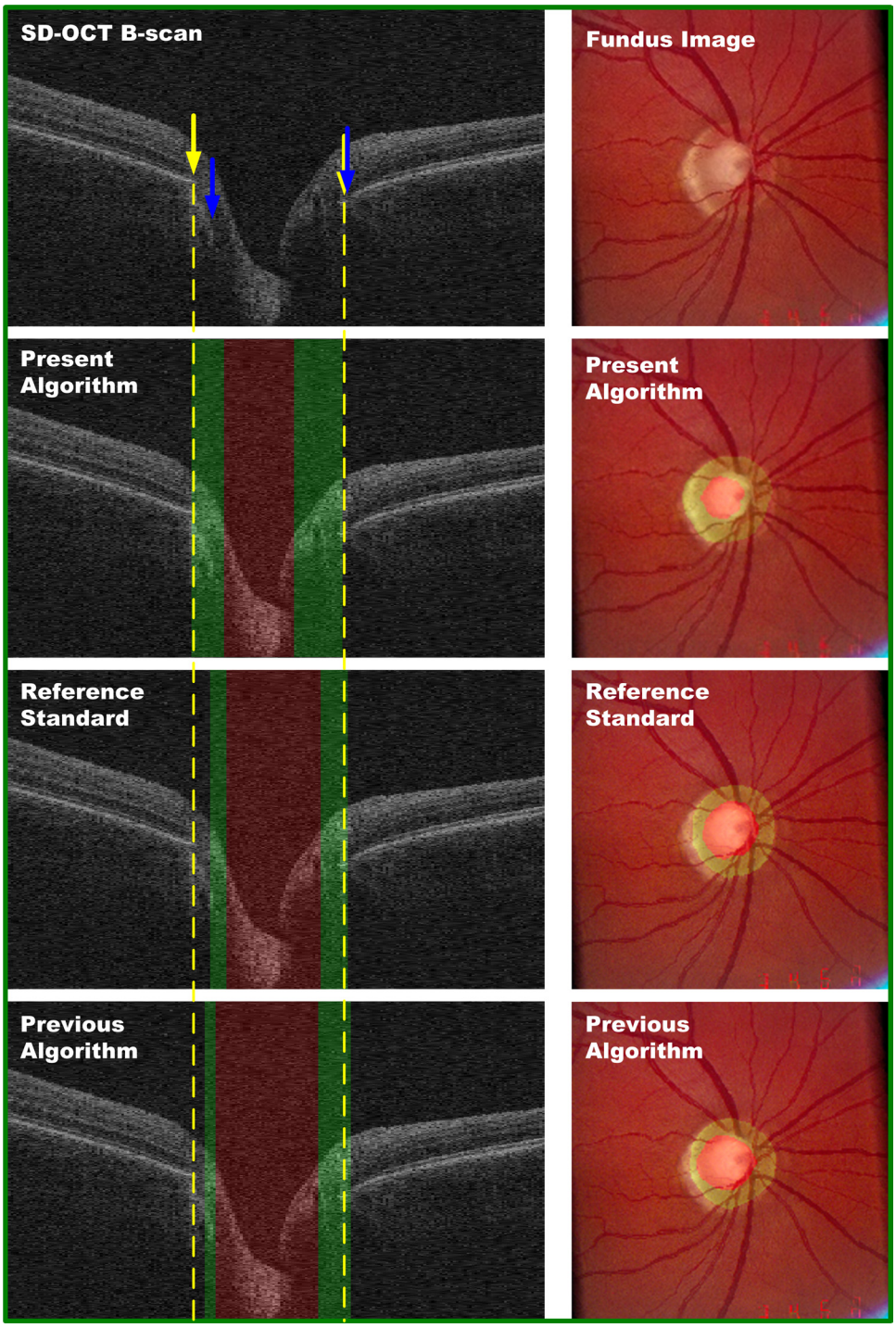

FIGURE 7. Comparison of present algorithm, expert, and previous algorithm segmentations with discrepancy. Raw SD-OCT and corresponding fundus image (*row 1*), present algorithm (*row 2*), RS (*row 3*), and previous algorithm (*row 4*) segmentations overlapping with raw SD-OCT and corresponding fundus image. SD-OCT central B-scan (*left*). Fundus image (*right*). *Yellow arrows*: position of the NCO from the algorithm (*dashed yellow line* indicates the projected NCO position). *Blue arrows*: clinical disc from the RS. *Green*, *red*: each method's projected rim and cup regions, respectively.

have larger biases than were found between the algorithm and the RS (as indicated by the signed errors in Table 1), this might have contributed to the larger unsigned errors as well. In addition, it is important to note that the definition of the algorithm's *cup boundary* is different from the traditional clinical definition of *cup margin*. The algorithm simply defined cup as the crossing point of the reference plane with the retinal surface, whereas the human experts tended to delineate the cup margin at the inflection point of the surface slope of the cup as seen in stereo photographs.[19] This may also explain our observation that cup area at the level of the RPE/BM plane was often smaller than the clinically visible cup area on stereo fundus photographs as seen by human experts (Fig. 3).

There are several advantages of the current automated segmentation approach over manual planimetry. First, although planimetry is the gold standard for quantifying glaucoma progression, it introduces great interobserver variability.[5] Its subjective nature is one of the potential sources of interobserver variability. However, the present automatic algorithm based on SD-OCT is completely objective and, therefore, should be more reproducible (assuming the NCO is a relatively stable landmark) compared with subjective, manual segmentation by human experts, though this has yet to be rigorously demonstrated. Second, as reported,[5] manual segmentation by planimetry is cumbersome and time-consuming and remains a research tool. However, the algorithm, when properly implemented, should

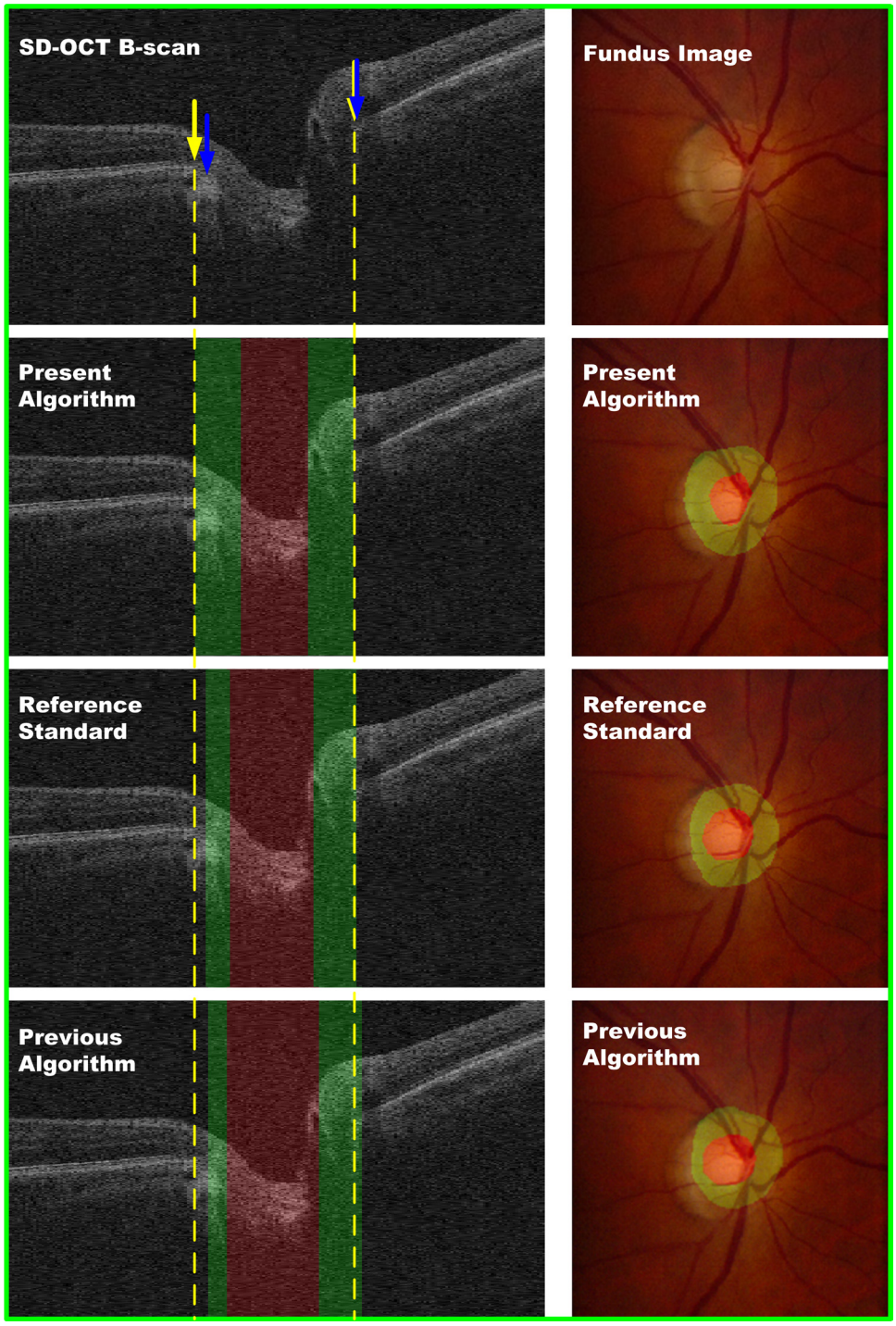

Figure 8. Comparison of present algorithm, expert, and previous algorithm segmentations with discrepancy. Raw SD-OCT and corresponding fundus image (*row 1*), present algorithm (*row 2*), RS (*row 3*), and previous algorithm (*row 4*) segmentations overlapping with raw SD-OCT and corresponding fundus image. SD-OCT central B-scan (*left*). Fundus image (*right*). *Yellow arrows*: position of the NCO from the algorithm (*dashed yellow line* indicates the projected NCO position). *Blue arrows*: clinical disc from the RS. *Green*, *red*: each method's projected rim and cup regions, respectively.

need only a few minutes to produce the analysis and would be compatible with that used in routine clinical use. Third, as found by our automated and others' manual [12,13,20] studies, the clinical optic disc margin seems to be the projection of a number of *different* recognizable anatomic landmarks, introducing greater variability between experts, depending on the landmarks they use to define "their" rim, and thus great variability for the quantification of glaucoma progression. Landmarks of the NCO will remain the same and, therefore, are expected to be relatively stable throughout the course of the glaucoma. An ideal reference plane based on a stable structure is critical in longitudinal imaging, glaucomatous analysis, and neuropathy analysis of the ONH. The NCO-based reference plane has the potential to more sensitively detect specific glaucomatous ONH changes, such as alterations in the anterior laminar surface and prelaminar neural tissue internal limiting membrane.[12,13] Although NCO-based metrics cannot replace the clinically appreciated optic disc margin, because the NCO is expected to be stable, it has the potential to provide a basis for other 2D or 3D ONH parameter quantification, and this would aid clinicians to more easily and better interpret the progression of glaucoma.

Thus, one of the major advantages of our present approach over our previous voxel classification approach[9] is that the present approach was able to segment natural ONH anatomic structures of NCO and optic cup at the RPE/BM complex to

enable all the advantages such structures may provide (such as the ability to compute 3D parameters based on a reference plane). In the previous approach, the RS from fundus photographs was used as truth in the training phase for the voxel classification and this resulted in mimicking the subjective assessment of the clinical defined optic disc margin and optic cup seen on photographs. As shown in the examples of Figure 7 and 8, although the segmentation of the previous approach closely corresponds to that of the RS, it does not overlap with a single constant structure in SD-OCT volumes. However, our core hypothesis—that segmentation of NCO will allow better estimation of glaucoma progression than the voxel classification-based approach—must be tested. This is possible only in a prospective study of sufficient duration.

There are several limitations to this preliminary study. One is that we used close to isotropic SD-OCT volumes. Potentially, a fully isotropic SD-OCT can lead to more accurate segmentation and corresponding parameter measurements. The 2D measurements of this work were not substantially influenced because they were computed on an isotropic X-Y plane. However, for future volumetric measurements, if applicable, it may be desirable to compute the volumetric parameters in the isotropic OCT space. Another was that the flattening of the raw SD-OCT greatly improved the motion artifacts and enabled us to compare the NCO-based 2D metrics with the 2D metrics of the clinical optic disc margin. However, this was not perfect, as shown in Figure 2. For the 2D measurements on the projection image, we corrected the nonoptimal flattening problem by extrapolating the average radial positions outside the estimated NCO with those inside it (see NCO and Optic Cup Segmentation at the RPE/BM Plane). For the volumetric measurements, it might have been necessary to transform the NCO-based reference plane back to the original raw SD-OCT space and to compute the volumetric parameters in the nonflattened isotropic space. Yet another is that, as reported,[21] with the glaucomatous damage of the lamina cribrosa and the peripheral scleral connective tissue, the cup enlarged and the NCO position might have changed relative to the peripheral sclera. Strouthidis et al.[12] suggested an alternative reference plane that was further from the center of the NCO boundary. This alternative reference plane could be obtained in a fixed distance from the segmented NCO and would have been less likely to deform posteriorly. Such change in reference plane position can be readily implemented in our algorithm, if desired.

In summary, we developed a novel automated graph-search-based machine algorithm to segment the NCO and optic cup at the level of RPE/BM complex in 3D OCT volumes of the ONH. In most eyes, the algorithm parameters correlated well with the RS parameters. However, a small discrepancy existed between the NCO and the clinical disc margin in some eyes. In addition, because of the relative stability of the NCO reference plane and the objective nature of the algorithm, we predict that the measurements of the NCO-based 2D or 3D glaucomatous parameters in volumetric OCT would be more reproducible than those of the RS parameters based on fundus photographs or even on the OCT parameters of the previous generation time-domain OCT. Additional work will be necessary to test our core hypothesis and to explore novel, objective, reproducible NCO-based parameters that correlate well with disease stage and progression.

Acknowledgments

The authors thank Claude F. Burgoyne and his research group from Devers Eye Institute for their helpful comments and discussion regarding histomorphometric and OCT based morphometric analysis of the ONH.

References

1. Bellezza AJ, Rintalan CJ, Thompson HW, et al. Deformation of the lamina cribrosa and anterior sclera canal wall in early experimental glaucoma. *Invest Ophthalmol Vis Sci.* 2003;44:623–637.
2. Schlamp CL, Li Y, Dietz JA, Janssen KT, Nickells RW. Progressive ganglion cell loss and optic nerve degeneration in DBA/2J mice is variable and asymmetric. *BMC Neurosci.* 2006;7:66.
3. Heijl A, Leske MC, Bengtsson B, Hyman L, Hussein M. Reduction of intraocular pressure and glaucoma progression: results from the Early Manifest Glaucoma Trial. *Arch Ophthalmol.* 2002;120:1268–1279.
4. Tielsch JM, Katz J, Quigley HA, Miller NR, Sommer A. Intraobserver and interobserver agreement in measurement of optic disc characteristics. *Ophthalmology.* 1998;95:350–356.
5. Kwon Y, Adix M, Zimmerman M, et al. Variance due to observer, repeat imaging, and fundus camera type on cup-to-disc ratio estimates by stereo planimetry. *J Glaucoma.* 2009;18:305–310.
6. Chauhan B, McCormick T, Nicolela M, LeBlanc R. Optic disc and visual field changes in a prospective longitudinal study of patients with glaucoma: comparison of scanning laser tomography with conventional perimetry and optic disc photography. *Arch Ophthalmol.* 2001;119:1492–1499.
7. Schuman J, Hee M, Puliafito C, et al. Quantification of nerve fiber layer thickness in normal and glaucomatous eyes using optical coherence tomography *Arch Ophthalmol.* 1995;113:586–596.
8. Drexler W, Fujimoto JG. State-of-the-art retinal optical coherence tomography. *Prog Retinal Eye Res.* 2008;27:45–88.
9. Abràmoff MD, Lee K, Niemeijer M, et al. Automated segmentation of the cup and rim from spectral domain OCT of the optic nerve head. *Invest Ophthalmol Vis Sci.* 2009;48:09–3790.
10. Abràmoff MD, Alward WL, Greenlee EC, et al. Automated segmentation of the optic nerve head from stereo fundus photographs using physiologically plausible feature detectors. *Invest Ophthalmol Vis Sci.* 2007;48:1665–1673.
11. Merickel M, Abràmoff MD, Sonka M, Wu X. Segmentation of the optic nerve head combining pixel classification and graph search. *Proc SPIE.* 2007;6512:651215.
12. Strouthidis N, Yang H, Fortune B, Downs J, Burgoyne C. Detection of the optic nerve head neural canal opening within three-dimensional histomorphometric and spectral domain optical coherence tomography data sets. *Invest Ophthalmol Vis Sci.* 2009;50:214–223.
13. Strouthidis N, Yang H, Reynaud JF, et al. Comparison of clinical and spectral domain optical coherence tomography optic disc margin. *Invest Ophthalmol Vis Sci.* 2009;50:4709–4718.
14. Garvin MK, Abràmoff MD, Wu X, Russell SR, Burns TL, Sonka M. Automated 3-D intraretinal layer segmentation of macular spectral-domain optical coherence tomography images. *IEEE Trans Med Imag.* 2009;28:1436–1447.
15. Lee K, Niemeijer M, Garvin MK, Kwon YH, Sonka M, Abràmoff MD. 3-D segmentation of the rim and cup in spectral-domain optical coherence tomography volumes of the optic nerve head. *Proc SPIE.* 2009;7262:72622D.
16. Garvin MK. *Automated 3-D Segmentation and Analysis of Retinal Optical Coherence Tomography Images* [dissertation]. Iowa City, IA: University of Iowa; 2008.
17. Li K, Wu X, Chen D, Sonka M. Globally optimal segmentation of interacting surfaces with geometric constraints. *Proc IEEE CS Conf CVPR.* 2004;1:394–399.
18. Hu Z, Niemeijer M, Lee K, Abràmoff MD, Sonka M, Garvin MK. Automated segmentation of the optic disc margin in 3-D optical coherence tomography images using a graph-theoretic approach. *Proc SPIE.* 2009;7262:72620U.
19. Kwon YH, Kim YI, Pereira ML, Montague PR, Zimmerman MB, Alward WL. Rate of optic disc cup progression in treated primary open-angle glaucoma. *J Glaucoma.* 2003;12:409–416.
20. Downs JC, Yang H, Girkin C, et al. Three dimensional histomorphometry of the normal and early glaucomatous monkey optic nerve head: neural canal and subarachnoid space architecture. *Invest Ophthalmol Vis Sci.* 2007;48:3195–3208.
21. Yang H, Downs JC, Girkin C, et al. 3-D Histomorphometry of the normal and early glaucomatous monkey optic nerve head: lamina cribrosa and peripapillary scleral position and thickness. *Invest Ophthalmol Vis Sci.* 2007;48:4597–4607.